Downloaded from www.rnajournal.org on February 14, 2006

Directed hydroxyl radical probing of 16S ribosomal RNA in ribosomes containing Fe(II) tethered to ribosomal protein S20

G. M. Culver and H. F. Noller

RNA 1998 4: 1471-1480

References

Article cited in:
http://www.rnajournal.org/cgi/content/abstract/4/12/1471#otherarticles

Email alerting service

Receive free email alerts when new articles cite this article - sign up in the box at the top right corner of the article or **click here**

Notes

To subscribe to *RNA* go to:
http://www.rnajournal.org/subscriptions/

© 1998 RNA Society

Downloaded from www.rnajournal.org on February 14, 2006

RNA (1998), *4*:1471–1480. Cambridge University Press. Printed in the USA.
Copyright © 1998 RNA Society.

Directed hydroxyl radical probing of 16S ribosomal RNA in ribosomes containing Fe(II) tethered to ribosomal protein S20

GLORIA M. CULVER and HARRY F. NOLLER

Center for Molecular Biology of RNA, Sinsheimer Laboratories, University of California, Santa Cruz, California 95064, USA

ABSTRACT

The 16S ribosomal RNA neighborhood of ribosomal protein S20 has been mapped, in both 30S subunits and 70S ribosomes, using directed hydroxyl radical probing. Cysteine residues were introduced at amino acid positions 14, 23, 49, and 57 of S20, and used for tethering 1-(*p*-bromoacetamidobenzyl)-Fe(II)-EDTA. In vitro reconstitution using Fe(II)-derivatized S20, together with the remaining small subunit ribosomal proteins and 16S ribosomal RNA (rRNA), yielded functional 30S subunits. Both 30S subunits and 70S ribosomes containing Fe(II)-S20 were purified and hydroxyl radicals were generated from the tethered Fe(II). Hydroxyl radical cleavage of the 16S rRNA backbone was monitored by primer extension. Different cleavage patterns in 16S rRNA were observed from Fe(II) tethered to each of the four positions, and these patterns were not significantly different in 30S and 70S ribosomes. Cleavage sites were mapped to positions 160–200, 320, and 340–350 in the 5′ domain, and to positions 1427–1430 and 1439–1458 in the distal end of the penultimate stem of 16S rRNA, placing these regions near each other in three dimensions. These results are consistent with previous footprinting data that localized S20 near these 16S rRNA elements, providing evidence that S20, like S17, is located near the bottom of the 30S subunit.

Keywords: 16S ribosomal RNA; directed hydroxyl radical probing; ribosomal protein S20

INTRODUCTION

The binding of ribosomal protein S20 to 16S ribosomal RNA (rRNA), or fragments of 16S rRNA, has been investigated by a variety of methods (Sogin et al., 1971; Daya-Grosjean et al., 1974; Muto et al., 1974; Zimmermann et al., 1974, 1975; Ungewickell et al., 1975; Ehresmann et al., 1977; Mackie & Zimmermann, 1978; Cormack & Mackie, 1991). Ribosomal protein S20 interacts with 16S rRNA stoichiometrically (Stöffler et al., 1971; Muto & Zimmermann, 1978) and independently of other proteins, defining it as a primary binding protein (Mizushima & Nomura, 1970; Held et al., 1974). These properties suggest that S20 plays a critical role in nucleating the assembly of the 30S subunit. While the gene encoding S20 is not essential, strains lacking S20 have a significantly reduced growth rate (Dabbs, 1979; Götz et al., 1989; Ryden-Aulin et al., 1993). Defects in posttranscriptional modification of 16S rRNA, in vivo 30S subunit assembly, translational fidelity, and subunit association have all been identified in cells lacking S20 (Dabbs, 1979; Götz et al., 1989; Ryden-Aulin et al., 1993).

Understanding the role of S20 in the ribosome is complicated not only by the multiple phenotypic effects observed in the deletion strain but also by discrepancies in the placement of S20 within the 30S subunit from different experimental approaches. Neutron diffraction mapping has placed S20 in the head of the 30S subunit, near S3 and S10 (Capel et al., 1987). In contrast, immunoelectron microscopy (IEM) has localized S20 near the bottom of the body of the 30S subunit, proximal to S17 and S15 (Schwedler et al., 1993). Footprinting studies using RNA-directed probes specific to either the base or sugar moieties have identified nucleotides near positions 190, 250, 270, and 320, all elements of the 5′ domain of 16S rRNA, as being some of the nucleotides protected by S20 (Stern et al., 1988a; Powers & Noller, 1995). Ribosomal protein S17 also protects some of these same nucleotides from modification with base-specific chemical probes (Stern et al., 1988a). This suggests that S17 and S20 are near one

Reprint requests to: Harry F. Noller, Center for Molecular Biology of RNA, Sinsheimer Laboratories, University of California, Santa Cruz, California 95064, USA; e-mail: harry@nuvolari.ucsc.edu.

Downloaded from www.rnajournal.org on February 14, 2006

another in the 30S subunit. Ribosomal protein S17 has been unambiguously positioned near the bottom of the body of the 30S subunit (Capel et al., 1987; Schwedler et al., 1993), thus it would follow that S20 should be positioned there too, consistent with its placement by IEM (Schwedler et al., 1993). Since the observed S20 footprints could either be due to direct protection of nucleotides at the S20 binding site or to indirect effects such as S20-induced structural rearrangements, we wished to directly survey the 16S rRNA environment proximal to S20 in the ribosome using directed hydroxyl radical probing.

Directed hydroxyl radical probing is a method for generating low resolution (10–50 Å; Joseph et al., 1997) information about the nucleic acid neighborhood in the vicinity of a defined site on a protein or nucleic acid. Previously, this approach has been used to study the 16S rRNA environment around individual ribosomal proteins in the 30S subunit (Heilek et al., 1995; Heilek & Noller, 1996a,b). Fe(II) is tethered to specific positions on the surface of a protein by reaction of the Fe(II)-loaded linker, 1-(*p*-bromoacetamidobenzyl)-EDTA (BABE; DeRiemer et al., 1981; Rana & Meares, 1991), with unique cysteine residues. The modified protein can then be incorporated into 30S subunits by reconstitution with 16S rRNA and the other 19 small subunit proteins (Traub & Nomura, 1968). Hydroxyl radicals are then produced locally by the Fenton reaction from the tethered Fe(II) (Dixon et al., 1991), cleaving the rRNA backbone of accessible nucleotides in the vicinity of the probe. This technique generates constraints for the three-dimensional folding of 16S rRNA elements. Additionally, Fe(II)-derivatized 30S subunits can be associated with natural 50S subunits to generate Fe(II)-derivatized 70S ribosomes. This allows for functional 30S subunits to be selected and probed; this probing data can be compared to that observed in free 30S subunits. Here we describe the use of this method to probe the 16S rRNA neighborhood around four positions on S20. Cleavage by Fe(II)-S20 was detected in the 5′ and 3′ minor domains of 16S rRNA; these results are in close agreement with previous footprinting studies, and are consistent with placement of S20 near the bottom of the body of the 30S subunit.

RESULTS

Construction of cysteine-containing mutants of S20

Single cysteine residues were introduced into *Escherichia coli* S20, which contains no cysteines in its wild-type sequence. Sites for cysteine substitution were chosen using an amino acid sequence alignment of S20 proteins from five organisms, targeting non-conserved residues likely to be found on the surface of the protein. Six sites for cysteine substitution, positions S14, S23, K49, I57, A72, and A77, were chosen out of the 86 amino acids of S20. The wild-type copy of the S20 gene was amplified by polymerase chain reaction (PCR) and cloned into pET24 (see Materials and Methods), which allows both overexpression of the recombinant protein as well as a means for generating single-stranded DNA for use in site-directed mutagenesis (Kunkel, 1985). Wild-type S20 and the six cysteine-containing S20 mutants were overexpressed, purified, and derivatized essentially as described for ribosomal protein S5 (Heilek & Noller, 1996b).

Footprinting Fe(II)-derivatized S20

The ability of the derivatized, mutant S20 proteins to confer the previously characterized S20 footprint on naked 16S rRNA (Stern et al., 1988a) was used to assess the proper folding of the recombinant protein, as well as the effects of the mutations and derivatization. Recombinant, wild-type S20 produces the same footprint as that observed for S20 purified from ribosomes either with (Fig. 1) or without (data not shown)

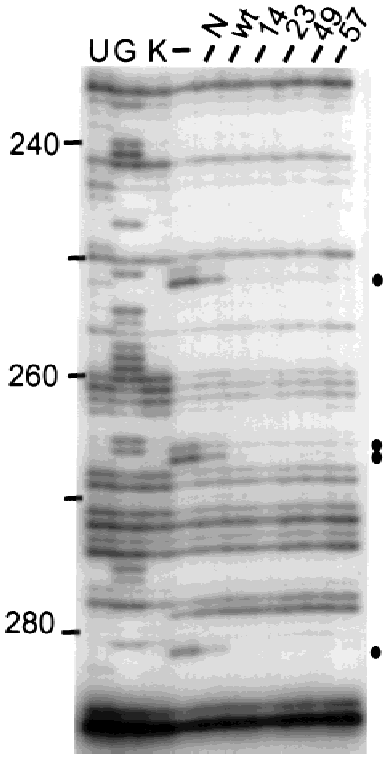

FIGURE 1. Protection of nucleotides in 16S rRNA from modification with kethoxal by Fe(II)-derivatized ribosomal protein S20. Primer extension analysis showing the 260 region of 16S rRNA using the 323 primer. U, G: sequencing lanes; K: unmodified 16S rRNA. RNA in all other lanes was treated with kethoxal following complex formation with (–) no protein; N: wild-type S20, isolated from ribosomes, treated in a mock reaction with Fe(II)-BABE; wt: recombinant wild-type S20 treated in a mock reaction with Fe(II)-BABE; 14: Fe-C14-S20; 23: Fe-C23-S20; 49: Fe-C49-S20; 57: Fe-C57-S20.

Downloaded from www.rnajournal.org on February 14, 2006

treatment with Fe(II)-BABE. The recombinant, wild-type protein affords complete protection of the RNA at a lower protein concentration than wild-type S20 isolated from ribosomes, suggesting that it contains a higher fraction of correctly folded protein (Fig. 1; data not shown). Four out of the six cysteine-containing mutants, Cys-14, Cys-23, Cys-49, and Cys-57, provide a footprint identical to wild-type S20 both with (Fig. 1) and without (data not shown) Fe(II)-derivatization. However, S20 substituted with cysteine at position 72 or 77, in the underivatized state, fails to protect any of the S20-specific nucleotides in 16S rRNA (data not shown), in agreement with previous S20 truncation experiments that implicate the C-terminus of S20 in binding to 16S rRNA (Donly & Mackie, 1988). These two mutants were not used in further experiments.

Reconstitution of 30S subunits with Fe(II)-derivatized S20

Although previous work showed that omission of S20 from in vitro 30S subunit reconstitution did not affect the sedimentation value of the reconstituted particles (Nomura et al., 1969), it was important to test whether derivatization of mutant S20 proteins would interfere with in vitro assembly. The derivatized proteins were reconstituted with 16S rRNA and the 19 other small subunit ribosomal proteins; formation of 30S subunits was monitored by sucrose gradient sedimentation (Fig. 2). Fe(II)-BABE derivatization has no significant effect on the sedimentation properties of subunits reconstituted with any of the four mutant proteins. In every case, peaks cosediment with that of natural 30S subunits (Fig. 2). The Fe(II)-S20 reconstitutions all give rise to smaller amounts of additional material that migrates more slowly than the major peak, most likely corresponding to partially folded or incompletely assembled particles.

Reconstituted 30S subunits assembled with Fe(II)-derivatized S20 are active in tRNA binding

While previous studies showed that 30S subunits reconstituted in the absence of S20 are competent for tRNA binding (Nomura et al., 1969), it was important to test whether Fe(II)-derivatization of mutant S20 proteins would interfere with tRNA binding. Fe(II)-derivatization of any of the four S20 mutant proteins had no significant effect on the ability of the reconstituted 30S subunits to bind tRNA in a poly(U)-dependent manner (Table 1). Some mRNA-independent binding of tRNA is also observed, consistent with the ionic conditions used for reconstitution, subsequent purification, and tRNA binding (Lill et al., 1986).

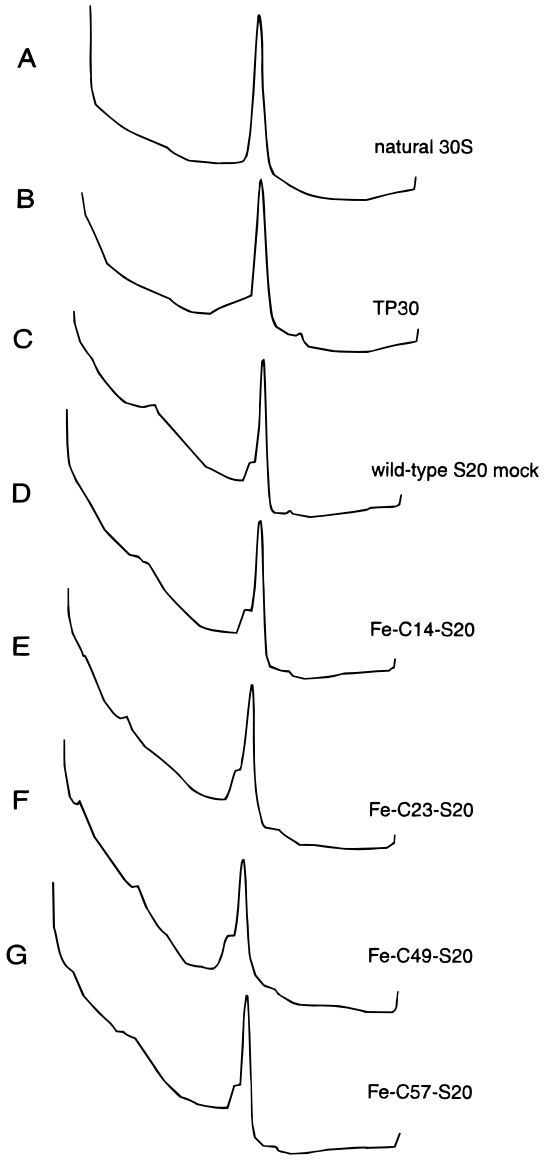

FIGURE 2. Sedimentation analysis of reconstituted 30S subunits using Fe(II)-BABE-derivatized S20 proteins. **A**: Natural 30S subunits. **B–G**: 30S subunits reconstituted with 16S rRNA and (**B**) TP30, (**C**) wild-type S20 treated in a mock reaction with Fe(II)-BABE, (**D**) Fe-C14-S20, (**E**) Fe-C23-S20, (**F**) Fe-C49-S20, (**G**) Fe-C57-S20. Sedimentation is from left to right, and absorbance was monitored at 254 nm.

Reconstituted 30S subunits assembled with Fe(II)-derivatized S20 are competent to form 70S ribosomes

E. coli strains that lack S20 produce subunits that are defective in subunit association (Dabbs, 1979; Götz et al., 1989; Ryden-Aulin et al., 1993). Therefore we wished to test the capacity of subunits containing Fe(II)-derivatized S20 to form 70S ribosomes. Subunits reconstituted with any of the four derivatized mutant S20 proteins were combined efficiently with 50S subunits to form 70S ribosomes (Fig. 3). Some small, slowly sed-

Downloaded from www.rnajournal.org on February 14, 2006

TABLE 1. tRNA binding activity of 30S subunits reconstituted with Fe(II)-S20

30S subunits	poly(U)-dependent $tRNA^{Phe}$ binding % activity	poly(U)-independent $tRNA^{Phe}$ binding % activity
Natural	100 ± 5	24 ± 3
Reconstituted with 16S rRNA		
+ TP30[a]	72 ± 4	19 ± 2
+ Σ mix[b]		
+ mock treated S20	54 ± 4	24 ± 4
+ Fe-C14-S20	57 ± 4	14 ± 2
+ Fe-C23-S20	48 ± 3	19 ± 3
+ Fe-C49-S20	54 ± 4	24 ± 2
+ Fe-C57-S20	62 ± 7	19 ± 3

Ribosomal subunits (5 pmol) were incubated with 10 pmol [^{32}P] $tRNA^{Phe}$ and 7.5 μg poly(U) (for poly(U)-dependent binding) in 50 μL of 20 mM $MgCl_2$, 100 mM KCl, 80 mM K^+-HEPES (pH 7.6) for 15 min at 37 °C followed by 10 min on ice. Binding of tRNA was assayed by filter binding (Nirenberg & Leder, 1964; Moazed & Noller, 1986). 100% activity corresponds to 0.5 pmol $tRNA^{Phe}$ bound/pmol ribosome.

[a]TP30: mixture of ribosomal proteins isolated from 30S subunits.

[b]Σ mix: stoichiometric mixture of individually purified recombinant 30S ribosomal proteins lacking S20.

imenting peaks are observed that contain material that does not associate with 50S subunits (Figs. 3E–3G). These peaks may contain incompletely assembled subunits, as suggested by the trailing shoulders observed in Figure 2.

Probing 30S subunits and 70S ribosomes with Fe(II)-derivatized S20

Both 30S subunits and 70S ribosomes containing S20 derivatized with Fe(II) at positions 14, 23, 49, and 57 (Fe-C14-S20, Fe-C23-S20, Fe-C49-S20, and Fe-C57-S20) were subjected to hydroxyl radical probing. Primer extension analysis identified cleavage of the rRNA backbone in two discrete regions of the 5′ domain and in the penultimate stem in the 3′ minor domain of 16S rRNA (Fig. 4). The target sites are classified based on band intensity, as visually compared to internal standards, and are summarized on the secondary structure of 16S rRNA in Figure 5. Overlapping cleavage is observed from Fe-C14-S20, Fe-C23-S20, and Fe-C57-S20, but with different intensities at different targets. Band intensities for Fe-C49-S20 are much weaker than those observed from the other three sites.

Target sites in the 5′ domain of 16S rRNA are localized to two discrete regions, around nucleotides 150–200 and 320–350 of 16S rRNA (Fig. 4A,B). Fe-C14-S20 and Fe-C23-S20 both cleave the RNA backbone at the 150 internal loop with similar intensities (Fig. 4A). The strongest cleavages in the 5′ domain are from Fe-C23-S20 on the 3′ strand of the 160 helix (Fig. 4A). This same strand of the 160 helix is targeted more weakly from position C14 (Fig. 4A). Nucleotides around 175 are targeted from Fe-C14-S20, Fe-C23-S20, and Fe-C57-S20 (Fig. 4A). The patterns of cleavage from positions C14 and C23 are similar in this region, while a stronger and slightly broader range of band intensities are observed from position C57 (Fig. 4A). The RNA backbone extending from the 3′ strand of the 190 helix and into the adjacent loop is cleaved by Fe-C57-S20 and considerably more weakly by Fe-C49-S20 (Fig. 4A).

A second region of the 5′ domain of 16S rRNA, between positions 320 and 350, is cleaved in three distinct patches by Fe-C14-S20 and Fe-C23-S20. Sites targeted by Fe-C57-S20 mirror those observed from Fe-C23-S20 although much more weakly (Fig. 4B). Nucleotides in both strands of the 320 helix as well as the 330 loop are cleaved by Fe-C14-S20 and Fe-C23-S20 (Fig. 4B). In this region only the 5′-most portion of the 330 loop is targeted by position C57. The strongest band intensities in this region of the 5′ domain of 16S rRNA are observed for position C14 in the 3′ strand of the 350 helix (Fig. 4B); in this region bands of weaker intensity are observed from positions C23 and C57.

Cleavage by Fe(II)-S20 in the penultimate stem in the 3′ minor domain of 16S rRNA is consistent with previous footprinting data (Stern et al., 1988a; Powers & Noller, 1995); target sites are observed in the two most distal internal loops of the penultimate stem and in the 5′ strand of the helix which connects them. Some of the most intense bands are observed for Fe-C14-S20 in the 1430 internal loop (Fig. 4C), with position C57 yielding less intense bands (Fig. 4C). Fe-C14-S20 and Fe-C23-S20 target sites in the 5′ strand of the 1440 helix (Fig. 4C). The internal loop near 1450 is cleaved by Fe-C57-S20 (Fig. 4C), while weaker cleavage is observed in this region from position C14. The 3′ side of the 1450 internal loop is targeted from posi-

Downloaded from www.rnajournal.org on February 14, 2006

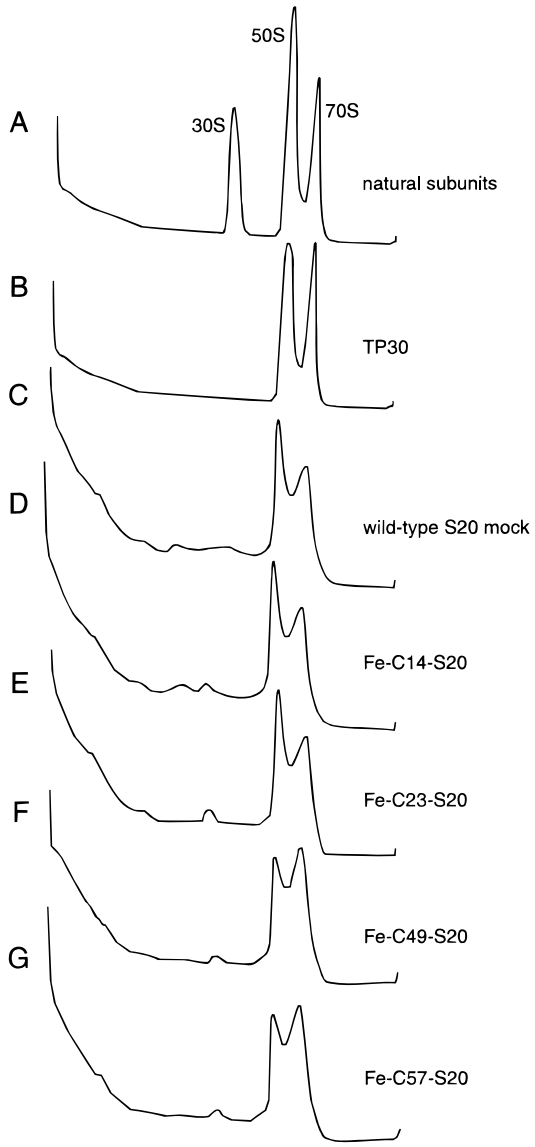

FIGURE 3. Sedimentation analysis of ribosomal subunit association using 30S subunits reconstituted in vitro with Fe(II)-BABE-derivatized S20 proteins. **A**: Natural 30S (30 pmol) and 50S (30 pmol) subunits incubated under conditions to yield a mixture of free subunits and 70S ribosomes. **B–G**: Full association of 50S subunits with 30S subunits reconstituted with (**B**) TP30, (**C**) wild-type S20 treated in a mock reaction with Fe(II)-BABE, (**D**) Fe-C14-S20, (**E**) Fe-C23-S20, (**F**) Fe-C49-S20, (**G**) Fe-C57-S20. Sedimentation is from left to right, and absorbance was monitored at 254 nm.

tion C57, with the strongest sites approaching 1460 (Fig. 4C). Fe-C49-S20 also targets sites in this internal loop, but more weakly than position C57 (Fig. 4C).

No significant detectable differences between the patterns of 16S rRNA cleavage in 30S subunits and 70S ribosomes were observed; the patterns and band intensities of all the target sites are very similar in 30S subunits and 70S ribosomes for all four Fe(II)-S20. An example is shown for the cleavage patterns observed in the penultimate stem, which are indistinguishable for 30S subunits (Fig. 4C, left panel) and 70S ribosomes (Fig. 4C, right panel).

DISCUSSION

Directed hydroxyl radical probing of the 16S rRNA environment in the vicinity of four different positions on ribosomal protein S20 targets two separate regions of the 5′ domain and the penultimate stem in the 3′ minor domain of 16S rRNA (Fig. 5). These data provide strong constraints for the three-dimensional folding of these RNA elements and for the location of ribosomal protein S20 in the 30S ribosomal subunit.

Ribosomal protein S20 is a primary binding protein; that is, it interacts specifically with 16S rRNA in the absence of other ribosomal proteins. Characterization of its binding site on 16S rRNA has been the subject of more than two decades of study (Sogin et al., 1971; Daya-Grosjean et al., 1974; Muto et al., 1974; Zimmermann et al., 1974, 1975; Ungewickell et al., 1975; Ehresmann et al., 1977; Rinke et al., 1977; Mackie & Zimmermann, 1978; Stern et al., 1988a; Cormack & Mackie, 1991; Powers & Noller, 1995). Along with S4 and S17, S20 is thought to be a critical component in organizing the 5′ domain of 16S rRNA. Also, it was shown that a fragment of 16S rRNA corresponding to the 5′ domain can form a discrete particle containing ribosomal proteins S4, S16, S17, and S20 (Weitzmann et al., 1993). S20 has been shown to bind and crosslink to RNA fragments contained within the 5′ end of 16S rRNA (Ehresmann et al., 1977, 1980; Rinke et al., 1977; Cormack & Mackie, 1991). Footprinting experiments have also localized S20 to the 5′ domain, as well as to the penultimate stem of 16S rRNA (Stern et al., 1988a; Powers & Noller, 1995; Fig. 5E,F). Hydroxyl radical footprinting using free Fe(II)-EDTA showed that S20 protects nucleotides 185–195, 330–335, 1434–1435, and 1447–1448 (Powers & Noller, 1995), in close agreement with the results of earlier base-specific chemical footprinting studies (Stern et al., 1988a). However, one major difference was found between the results of the two different footprinting studies. Base-specific footprinting showed protection of the 240–280 region by both S17 and S20 (Stern et al., 1988a; Fig. 5E), while a hydroxyl radical footprint was found for this region only with S17 (Powers & Noller, 1995; Fig. 5F). Most of these previous studies have focused on the interaction of S20 with 16S rRNA, or fragments of 16S rRNA, whereas the directed hydroxyl radical probing has been performed in 30S subunits and 70S ribosomes and may more accurately reflect the RNA environment of S20 in the fully assembled 30S subunit. The results presented here, using directed hydroxyl radical probing from Fe(II) tethered to S20 (Figs. 5A–5D) show no cleavage in the 240–280 region of 16S rRNA, consistent with the hydroxyl radical footprinting data (Powers & Noller, 1995). The ab-

Downloaded from www.rnajournal.org on February 14, 2006

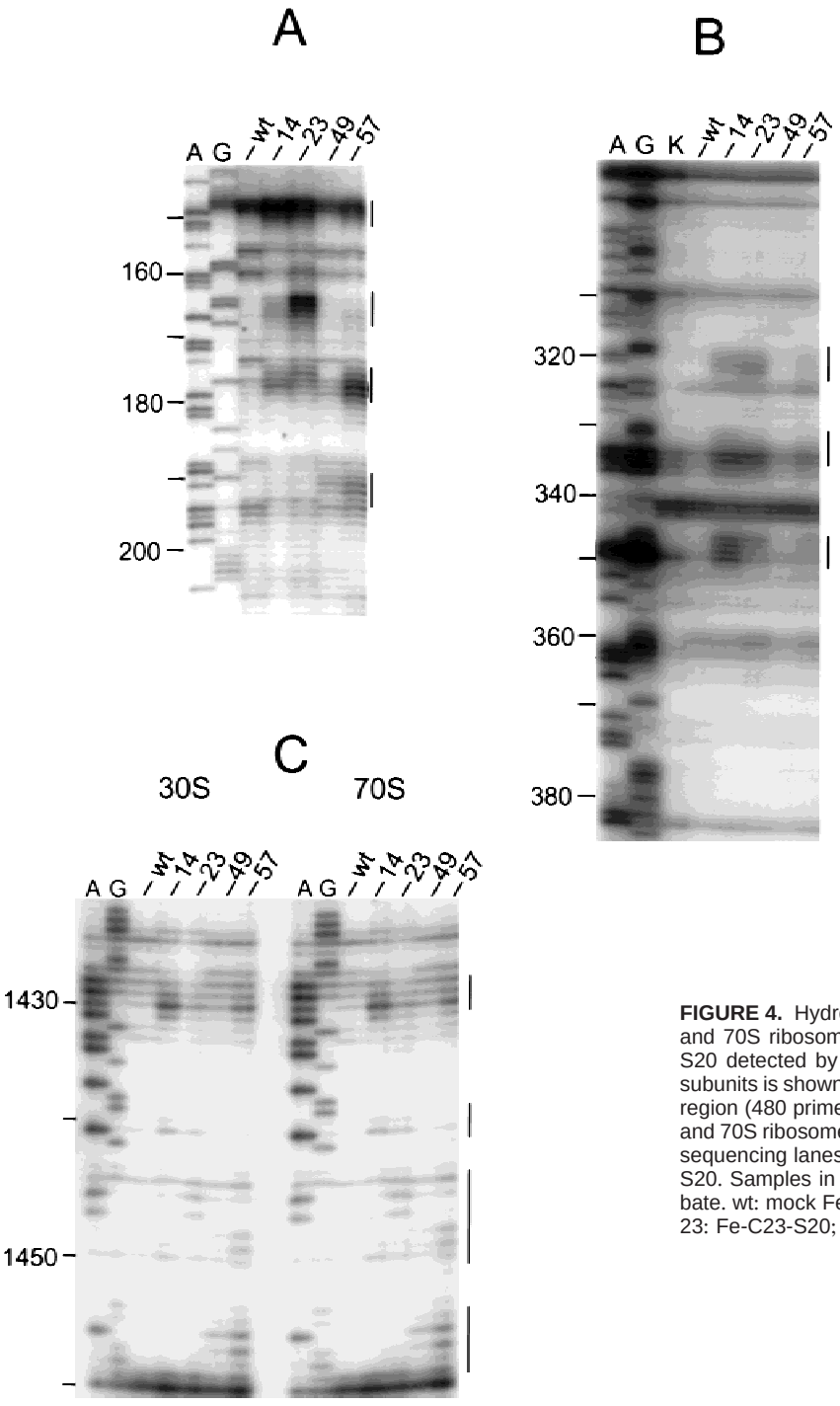

FIGURE 4. Hydroxyl radical cleavage of 16S rRNA in 30S subunits and 70S ribosomes containing Fe(II)-derivatized ribosomal protein S20 detected by primer extension. Cleavage of 16S rRNA in 30S subunits is shown for (**A**) the 180 region (232 primer) and (**B**) the 340 region (480 primer). **C:** Cleavage of 16S rRNA in both 30S subunits and 70S ribosomes is shown for the 1430 region (1490 primer). A, G: sequencing lanes; K: unprobed mock Fe(II)-BABE-treated wild-type S20. Samples in all other lanes were treated with H_2O_2 and ascorbate. wt: mock Fe(II)-BABE-treated wild-type S20; 14: Fe-C14-S20; 23: Fe-C23-S20; 49: Fe-C49-S20; 57: Fe-C57-S20.

sence of cleavage in this region of 16S rRNA could be due to the lack of derivatization of a position on S20 that is in the vicinity of this helix. Alternatively, it is possible that the S20 base-specific footprint observed on naked 16S rRNA (Stern et al., 1988a; Fig. 1) is either indirect or not sustained throughout 30S subunit assembly. This latter suggestion would be in agreement with our data and the interpretation that the 260 helix is the primary binding site for S17, not S20 (Stern et al., 1988a).

Proximity of S20 to the same three regions of 16S rRNA that were footprinted by chemical probes (Stern et al., 1988a; Powers & Noller, 1995), provides additional evidence that S20 interacts with these three regions of the RNA in 30S subunits. Because of the small size of S20 (86 amino acids) these three structural regions of 16S rRNA must be close to one another. Since the 5′ domain is the first domain of 16S rRNA to be transcribed, S20, as a primary binding protein, may

Downloaded from www.rnajournal.org on February 14, 2006

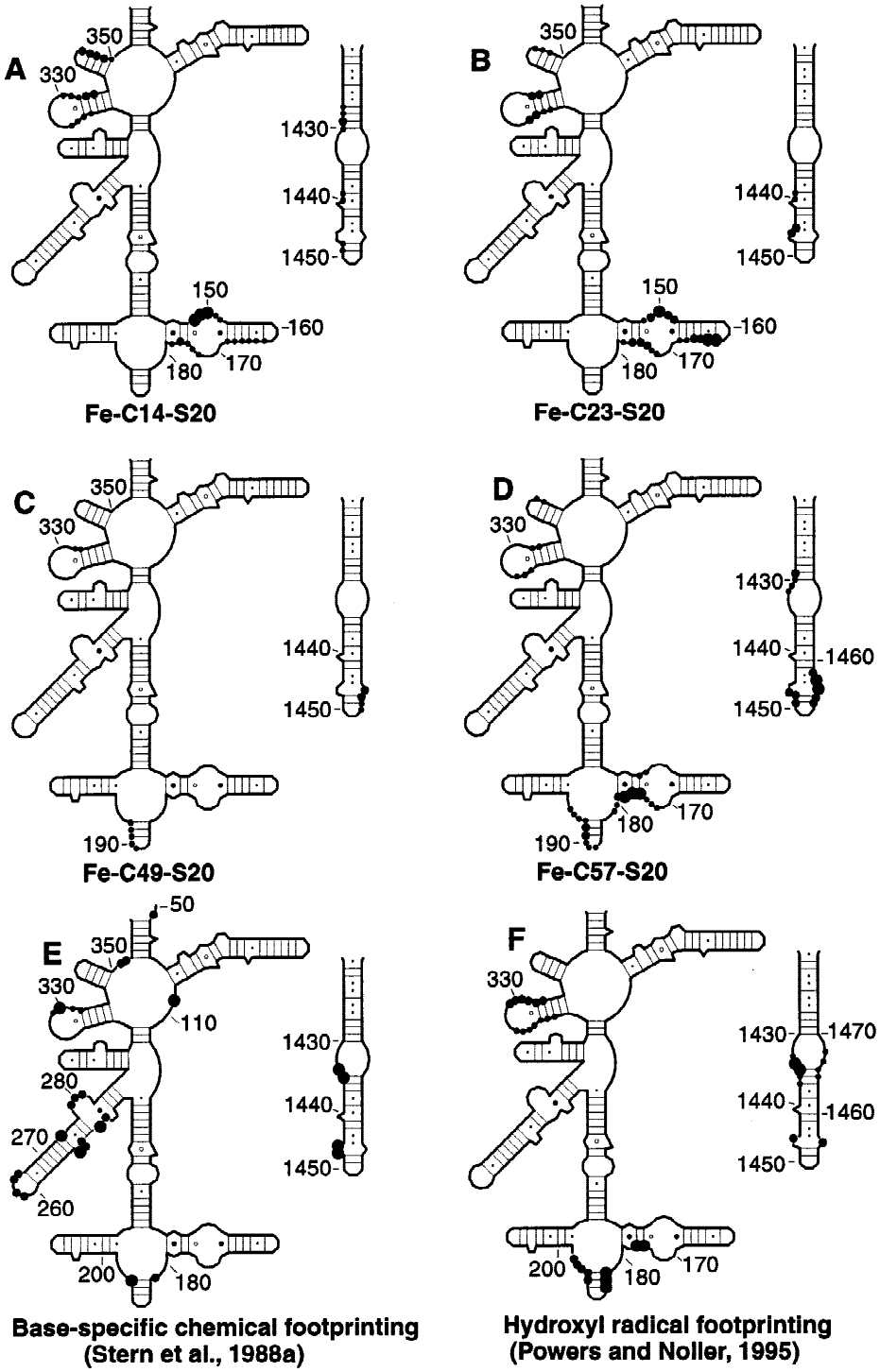

FIGURE 5. Secondary structure of elements of the 5′ domain and the penultimate stem of 16S rRNA, summarizing the sites of directed hydroxyl radical cleavage from Fe(II)-derivatized S20 mutant proteins. Filled circles indicate positions of cleavage in 30S subunits and 70S ribosomes reconstituted with (**A**) Fe-C14-S20; (**B**) Fe-C49-S20; (**C**) Fe-C49-S20; (**D**) Fe-C57-S20. Also shown are results of S20 footprinting experiments using (**E**) base-specific chemical probes (Stern et al., 1988a) and (**F**) hydroxyl radicals generated from free Fe(II)-EDTA (Powers & Noller, 1995). The intensities of the observed cleavages or protections were classified based on visual comparison to internal standards and are reflected in the sizes of the filled circles.

help to nucleate 30S subunit assembly and stabilize important intramolecular RNA interactions. This idea is consistent with experiments studying the dynamics of in vitro assembly of 30S subunits (Powers et al., 1993) which show that different regions of 16S rRNA fold at different rates. The nucleotides in the 5′ domain that are protected by S20 belong to the fastest kinetic class and thus are likely to be involved in the early stages of

Downloaded from www.rnajournal.org on February 14, 2006

assembly. This is also consistent with previous work which demonstrated that S20 interacts strongly with fragments of 16S rRNA corresponding to only the 5′ end (Ehresmann et al., 1977, 1980; Rinke et al., 1977; Cormack & Mackie, 1991). Our data also provide new evidence for the interaction of S20 with the penultimate stem, near the 3′ end of 16S rRNA in 30S subunits. This leads to the interesting possibility that S20 acts to stabilize interactions between the penultimate stem and the 5′ domain of 16S rRNA, indicating a potential role for S20 in both early and late events of ribosome assembly.

There is interesting overlap in the data from directed hydroxyl radical probing from Fe(II) tethered to S20 and previous S20 footprinting results (Stern et al., 1988a; Powers & Noller, 1995). Some of the 16S rRNA nucleotides which are protected by S20 in footprinting experiments are also cleaved by Fe(II)-derivatized S20 (Fig. 5). Nucleotides near 180, and in the 190 and 330 helices are both cleaved and footprinted by S20, as are the most distal nucleotides in the penultimate stem (Fig. 5). This is an interesting observation since the more expected result would be cleavage of nucleotides adjacent to those which are protected, as is seen near 1430 (Fig. 5). It is possible that some of the S20 footprints are indirect and that the observed protections are due to altered conformations, and therefore altered availability, of the nucleotides. Thus, probing from Fe(II)-derivatized S20 would result in cleavage of the same nucleotides which are protected. Since derivatization of all four mutant S20 proteins does not alter the characteristic footprints, it is possible that the probing sites are adjacent to residues responsible for the footprint and thus, the two independent methods could result in sampling of the same environment. It is also possible that the observed overlap from the two techniques is the result of different conformations of 16S rRNA. The footprinting experiments were performed on naked 16S rRNA (Stern et al., 1988a; Powers & Noller, 1995), while the directed hydroxyl radical probing was performed on fully assembled 30S subunits. Thus, the interaction of S20 with 16S rRNA may vary at different stages of assembly. This possibility alone or in combination with those offered above could account for the overlap between the footprinting and directed hydroxyl radical probing data.

In the absence of a three-dimensional structure for ribosomal protein S20, detailed modeling of its interaction with 16S rRNA is precluded. Nevertheless, some clues regarding the interactions are suggested by our data. Because of the small size of S20 and the observed overlap in the cleavage targets from the four probing positions, it is possible that the observed cleavage targets provide a comprehensive picture of the 16S rRNA environment of S20, with the possible exception of its C-terminal region. We were unable to substitute cysteine residues in the C-terminus of S20 without disruption of binding, consistent with previous work implicating this region of the protein in rRNA binding (Donly & Mackie, 1988). The weak cleavage observed from Fe-C49-S20 is most easily explained by its orientation away from RNA targets, because its binding does not appear to be impaired (Fig. 1). Fe-C14-S20 and Fe-C23-S20 cleave only one face of the helix ranging from 150–180, suggesting that the opposite face of the helix is protected by other interactions. Cleavage patterns in two distinct regions suggest juxtaposition of S20 with the minor groove of two different helices; Fe-C14-S20 produces a 3′-staggered cleavage in the 320/330 helix, as does Fe-C57-S20 in the 1450–1460 region. These data suggest potential modes of interaction between S20 and 16S rRNA.

The data presented here have significant bearing on conflicting reports concerning the three-dimensional location of S20 in the 30S subunit. Neutron mapping experiments have placed S20 in the head of the 30S subunit, near ribosomal proteins S3 and S10 (Capel et al., 1987). In contrast, S20 has been localized near the bottom of the body of the subunit by IEM studies (Schwedler et al., 1993). The IEM data locate S20 proximal to S17, consistent with conclusions drawn from footprinting experiments (Stern et al., 1988a; Powers & Noller, 1995) and with the directed probing results presented here. Both IEM and neutron diffraction studies localized S17 to the bottom of the body of the 30S subunit (Capel et al., 1987; Schwedler et al., 1993). The RNA regions in the 5′ domain that are targeted by Fe(II)-derivatized S20 directly flank RNA elements that are cleaved by Fe(II)-S17 (G.M. Heilek & H.F. Noller, unpubl. results) and Fe(II)-S15 (G.M. Culver & H.F. Noller, unpubl.). Taken together, the data are most consistent with the placement of S20 near the bottom of the body of the 30S subunit.

MATERIALS AND METHODS

Reagents

Preparation of 16S rRNA, 30S, 50S, and 70S ribosomes was as described (Moazed & Noller, 1986). Synthesis of BABE and preparation of the Fe(II)-BABE complex were done as previously described (DeRiemer et al., 1981). Buffer A consists of 80 mM K^+-HEPES (pH 7.6), 20 mM $MgCl_2$, 330 mM KCl, and 0.01% Nikkol.

Cloning, expression and purification of ribosomal protein S20

The gene encoding ribosomal protein S20 was amplified by PCR of *E. coli* MRE600 genomic DNA with restriction sites included in the DNA primers for convenient cloning: primer #1, 5′ end of the S20 gene with *Nde*I restriction enzyme site (underlined), GGGGCGCGGATCCCATATGGCTTAT ATCAAATCAGCTAAG; primer #2, 3′ end of the S20 gene

Downloaded from www.rnajournal.org on February 14, 2006

with *Hin*dIII restriction enzyme site (underlined), GGCGGGAAGCTTTTAAGCCAGTTTGTTGATCTGTGC. PCR products were cleaved with *Nde*I and *Hin*dIII and ligated into identically restricted pET24b (Novagen). Restriction enzyme digestion and DNA sequence analysis was used to identify wild-type S20 clones. Single stranded DNA was produced directly from the wild-type construct, and cysteines were introduced at six sites (14, 23, 49, 57, 71, and 74) by site-directed mutagenesis (Kunkel, 1985). Wild-type and mutant S20 proteins were overexpressed from an inducible T7 RNA polymerase promoter in the pET24b vector (Studier et al., 1990). S20 proteins were purified by FPLC cation exchange chromatography on a Resource S (Pharmacia) column run at 4 °C in 6 M Urea, 20 mM K^+-HEPES (pH 7.0) with a 120 mL elution gradient from 20–400 mM KCl with S20 eluting at 160 mM.

Derivatization of S20 proteins

Conjugation of Fe(II)-BABE to cysteine-containing mutants of S20 and purification of derivatized proteins from unreacted reagent was done essentially as described (Heilek et al., 1995); 2 nmol protein in 80 mM K^+-HEPES (pH 7.7), 1 M KCl, and 1 mM *B*-mercaptoethanol were incubated with 100 nmol Fe(II)-BABE in 100 μL buffer containing 80 mM K^+-HEPES (pH 7.7), 1 M KCl, and 0.01% Nikkol (Nikko Chemicals, Japan) at 37 °C for 30 min. Free Fe(II)-BABE was separated from derivatized protein on Microcon 3 microconcentrators using multiple washes with a buffer containing 80 mM K^+-HEPES (pH 7.7), 1 M KCl, and 0.01% Nikkol. Wild-type S20, which contains no cysteines, was treated identically to the cysteine-containing mutants in mock reactions to control for possible derivatization of non-cysteine side chains.

Footprinting S20 on naked 16S rRNA

Complexes of 16S rRNA and S20 were formed and probed with kethoxal essentially as described by Stern et al. (1988a). Briefly, 20 μg of 16S rRNA was incubated at 42 °C for 60 min with a fivefold molar excess of Fe(II)-S20 in buffer A. Control samples of 16S rRNA alone were treated identically to those containing protein. After incubation at 42 °C, samples were incubated at 0 °C for 10 min. For kethoxal modification, 4 μL of kethoxal (37 mg/mL) were added to each 100-μL sample followed by incubation at 0 °C for 60 min. Samples were adjusted to, and maintained at, 25 mM K^+-borate (pH 7.0). Samples were precipitated with 2.5 volumes of ethanol and 0.1 volume 3 M sodium acetate (pH 5.2). RNA was isolated and analyzed by primer extension as previously described (Stern et al., 1988b).

Reconstitution of 30S subunits and subunit association

Reconstitution of 30S particles was done using sequential addition of a four-fold molar excess of purified recombinant proteins (S2–S21) to 16S rRNA following the ordered assembly pathway (Traub & Nomura, 1968; Held et al., 1974; G.M. Culver & H.F. Noller, submitted). Reconstituted 30S subunits were purified from unincorporated proteins by centrifugation in Microcon 100 microconcentrators at 3,000 rpm for 5 min with three consecutive washes of 400 μL each with Buffer A (80 mM K^+-HEPES (pH 7.6), 20 mM $MgCl_2$, 330 mM KCl, and 0.01% Nikkol). Reconstituted 30S subunits were incubated with natural 50S subunits in 80 mM K^+-HEPES (pH 7.6), 20 mM $MgCl_2$, 100 mM KCl, and 0.003% Nikkol at 37 °C for 30 min.

Purification of 30S subunits and 70S ribosomes

Wild-type or Fe(II)-derivatized S20 containing 30S subunits or 70S ribosomes were purified by sedimentation through a 10–40% sucrose gradient (in 20 mM K^+-HEPES (pH 7.6), 20 mM $MgCl_2$, and 100 mM KCl) at 32,000 rpm (SW41) for 15.5 h at 4 °C. Sucrose was removed from 30S subunits and 70S ribosomes by centrifugation at 4 °C for 60 min at 2,400 rpm (JA20) in Centricon 100 ultraconcentrators with 3–4 sequential 2.0 mL washes with buffer A.

Hydroxyl radical probing and primer extension

Isolated 30S and 70S ribosomes were probed by initiating hydroxyl radical formation with 0.05% H_2O_2 and 5 mM ascorbic acid, and incubated for 10 min on ice. One-third volume of thiourea (20 mM) was added to quench the reaction. Samples were precipitated with 2.5 volumes of ethanol and 0.1 volume 3 M sodium acetate (pH 5.2). RNA was isolated and analyzed by primer extension as previously described (Stern et al., 1988b).

ACKNOWLEDGMENTS

We thank Lovisa Holmberg, Kate Lieberman, and Lisa Newcomb for critical comments on the manuscript; J. Moran, D.P. Greiner, and S. Joseph for 1-(*p*-bromoacetamidobenzyl)-EDTA, which was synthesized in the laboratory of Claude Meares. This work was supported by NIH Grant No. GM-17129 (to H.F.N.), NIH post-doctoral fellowship No. 1FM32GM18065-01 (to G.M.C.) and a grant to the Center for the Molecular Biology of RNA from the Lucille P. Markey Charitable Trust.

Received July 9, 1998; returned for revision August 6, 1998; revised manuscript received August 25, 1998

REFERENCES

Capel MA, Engelman DM, Freeborn BR, Kjeldgaard M, Langer JA, Ramakrishnan V, Schindler DG, Schneider DK, Schoenborn BP, Sillers I-Y, Yabuki S, Moore PB. 1987. A complete mapping of the proteins in the small ribosomal subunit of *Escherichia coli*. *Science 238*:1403–1406.

Cormack RS, Mackie GA. 1991. Mapping ribosomal protein S20-16S rRNA interactions by mutagenesis. *J Biol Chem 266*:18525–18529.

Dabbs ER. 1979. Selection for *Escherichia coli* mutants with proteins missing from the ribosome. *J Bact 140*:734–737.

Daya-Grosjean L, Reinbolt J, Pongs O, Garrett RA. 1974. A study of the regions of ribosomal proteins S4, S8, S15, S20 that interact with 16S RNA of *Escherichia coli*. *FEBS Lett 44*:253–256.

DeRiemer LH, Meares CF, Goodwin DA, Diamanti CJ. 1981. BLEDTA-II synthesis of a new tumor-visualizing derivative of Co(II)-bleomycin. *J Labeled Compd Radiopharm 18*:1517–1534.

Downloaded from www.rnajournal.org on February 14, 2006

Dixon WJ, Hayes JJ, Levin JR, Weidner MF, Dombroski BA, Tullius TD. 1991. Hydroxyl radical footprinting. *Methods Enzymol 208*:380–413.

Donly BC, Mackie GA. 1988. Affinities of ribosomal protein S20 and C-terminal deletion mutants for 16S rRNA and S20 mRNA. *Nucleic Acids Res 16*:997–1010.

Ehresmann B, Backendorf C, Ehresmann C, Ebel JP. 1977. Characterization of the regions from *E. coli* 16S RNA covalently linked to ribosomal proteins S4 and S20 after ultraviolet irradiation. *FEBS Lett 78*:261–266.

Ehresmann C, Stiegler P, Carbon P, Ungewickell E, Garrett RA. 1980. The topography of the 5′ end of 16S RNA in the presence and absence of ribosomal proteins S4 and S20. *Eur J Biochem 103*:439–446.

Götz F, Fleischer C, Pon CL, Gualerzi CO. 1989. Subunit association defects in *Escherichia coli* ribosome mutants lacking proteins S20 and L11. *Eur J Biochem 183*:19–24.

Heilek GM, Marusak R, Meares CF, Noller HF. 1995. Directed hydroxyl radical probing of 16S rRNA using Fe(II) tethered to ribosomal protein S4. *Proc Natl Acad Sci USA 92*:1113–1116.

Heilek GM, Noller HF. 1996a. Directed hydroxyl radical probing of the rRNA neighborhood of ribosomal protein S13 using tethered Fe(II). *RNA 2*:597–602.

Heilek GM, Noller HF. 1996b. Site-directed hydroxyl radical probing of the rRNA neighborhood of ribosomal protein S5. *Science 272*:1659–1662.

Held WA, Ballou B, Mizushima S, Nomura M. 1974. Assembly mapping of 30S ribosomal proteins from *Escherichia coli*. *J Biol Chem 249*:3103–3111.

Joseph S, Weiser B, Noller HF. 1997. Mapping the inside of the ribosome with an RNA helical ruler. *Science 278*:1093–1098.

Kunkel TA. 1985. Rapid and efficient site-specific mutagenesis without phenotypic selection. *Proc Natl Acad Sci USA 82*:488–492.

Lill R, Robertson JM, Wintermeyer W. 1986. Affinities of tRNA binding sites of ribosomes from *Escherichia coli*. *Biochemistry 25*: 3245–3255.

Mackie GA, Zimmermann RA. 1978. RNA–protein interactions in the ribosome IV. Structure and properties of binding sites for proteins S4, S16/S17 and S20 in the 16S RNA. *J Mol Biol 121*:17–39.

Mizushima S, Nomura M. 1970. Assembly mapping of 30S ribosomal proteins in *E. coli*. *Nature 226*:1214–1218.

Moazed D, Noller HF. 1986. Transfer RNA shields specific nucleotides in 16S ribosomal RNA from attack by chemical probes. *Cell 47*:985–994.

Muto A, Ehresmann C, Fellner P, Zimmermann RA. 1974. RNA–protein interactions in the ribosome. I. Characterization and ribonuclease digestion of 16S RNA-ribosomal protein complexes. *J Mol Biol 86*:411–432.

Muto A, Zimmermann RA. 1978. RNA–protein interactions in the ribosome. III. Conformation and stability of ribosomal protein binding sites in the 16S rRNA. *J Mol Biol 121*:1–15.

Nirenberg M, Leder P. 1964. RNA code words and protein synthesis. *Science 145*:1399–1407.

Nomura M, Mizushima S, Ozaki M, Traub P, Lowry CV. 1969. Structure and function of ribosomes and their molecular components. *Cold Spring Harb Symp Quant Biol 34*:49–61.

Powers T, Daubresse G, Noller HF. 1993. Dynamics of in vitro assembly of 16S rRNA into 30S ribosomal subunits. *J Mol Biol 232*:362–374.

Powers T, Noller HF. 1995. Hydroxyl radical footprinting of ribosomal proteins on 16S rRNA. *RNA 1*:194–209.

Rana TM, Meares CF. 1991. Transfer of oxygen from an artificial protease to peptide carbon during proteolysis. *Proc Natl Acad Sci USA 88*:10578–10582.

Rinke J, Ross A, Brimacombe R. 1977. Characterisation of RNA fragments obtained by mild nuclease digestion of 30S ribosomal subunits from *Escherichia coli*. *Eur J Biochem 76*:189–196.

Ryden-Aulin M, Shaoping Z, Kylsten P, Isaksson LA. 1993. Ribosome activity and modification of 16S RNA are influenced by deletion of ribosomal protein S20. *Mol Microbiol 7*:983–992.

Schwedler G, Albrecht-Ehrlich R, Ark K-H. 1993. Immunoelectron microscopic localization of ribosomal proteins BS8, BS9, BS20, BLl3, and BL21 on the surface of 30S and 50S subunits from *Bacillus stearothermophilus*. *Eur J Biochem 217*:361–369.

Sogin M, Pace B, Pace NR, Woese CR. 1971. Primary structural relationship of p16 to m16 ribosomal RNA. *Nature New Biol 232*:48–49.

Stern S, Changchien L-M, Craven GR, Noller HF. 1988a. Interaction of proteins S16, S17, and S20 with 16S ribosomal RNA. *J Mol Biol 200*:291–299.

Stern S, Moazed D, Noller HF. 1988b. Structural analysis of RNA using chemical and enzymatic probing monitored by primer extension. *Methods Enzymol 164*:481–489.

Stöffler G, Daya L, Ark KH, Garrett RA. 1971. Ribosomal proteins. XXVI. The number of specific protein binding sites on 16S and 23S RNA of *Escherichia coli*. *J Mol Biol 62*:411–414.

Studier FW, Rosenberg AH, Dunn JJ, Dubendorff JW. 1990. Use of T7 RNA polymerase to direct expression of cloned genes. *Methods Enzymol 185*:60–89.

Traub P, Nomura M. 1968. Structure and function of *E. coli* ribosomes, V. Reconstitution of functionally active 30S ribosomal particles from RNA and proteins. *Proc Natl Acad Sci USA 59*:777–784.

Ungewickell E, Garrett R, Ehresmann C, Stiegler P, Fellner P. 1975. An investigation of the 16S RNA binding sites of ribosomal proteins S4, S8, S15, S20 from *Escherichia coli*. *Eur J Biochem 51*:165–180.

Weitzmann CJ, Cunningham PR, Nurse K, Ofengand J. 1993. Chemical evidence for domain assembly of the *Escherichia coli* 30S ribosome. *FASEB J 7*:177–180.

Zimmermann RA, Mackie GA, Muto A, Garrett RA, Ungewickell E, Ehresmann C, Stiegler P, Ebel JP, Fellner P. 1975. Location and characteristics of ribosomal protein binding sites in the 16S RNA of *Escherichia coli*. *Nucleic Acids Res 2*:279–302.

Zimmermann RA, Muto A, Mackie GA. 1974. RNA–protein interactions in the ribosome. II. Binding of ribosomal proteins to isolated fragments of the 16S RNA. *J Mol Biol 86*:433–450.